Evidence for shifting regional moisture imbalances from isotope ratios in water vapor

A. Bailey, Joint Institute for the Study of the Atmosphere and Ocean, University of Washington, Seattle, Washington, USA. Now at Department of Earth Sciences, Dartmouth College, Hanover, New Hampshire, USA.

P. N. Blossey, Department of Atmospheric Sciences, University of Washington, Seattle, Washington, USA.

D. Noone, College of Earth, Ocean, and Atmospheric Sciences, Oregon State University, Corvallis, Oregon, USA.

J. Nusbaumer, Cooperative Institute for Research in Environmental Sciences and Department of Atmospheric and Oceanic Sciences, University of Colorado Boulder, Boulder Colorado, USA; now at NASA Goddard Institute for Space Studies, New York, NY, USA.

R. Wood, Department of Atmospheric Sciences, University of Washington, Seattle, Washington, USA.

Corresponding author: A. Bailey, Department of Earth Sciences, Dartmouth College, 6105 Fairchild Hall, Hanover, NH 03755, USA. (adriana@dartmouth.edu)

Key Points

Isotopic anomalies with respect to water vapor concentration are defined

Observed and simulated anomalies track variations in moisture flux divergence

This sensitivity implies the ability to track future hydroclimate variability

Abstract

As global temperatures rise, regional differences in evaporation (*E*) and precipitation (*P*) are likely to become more disparate, causing the drier *E*-dominated regions of the tropics to become drier and the wetter *P*-dominated regions to become wetter. However, monitoring these changes is challenging due to the inherent difficulties of measuring *E* and *P* with sufficient spatial coverage and temporal resolution. This work demonstrates that isotope ratios in water vapor are a powerful tracer of changes in hydroclimate variability due to their sensitivity to regional moisture imbalances. Using remotely sensed isotope ratios derived from NASA's Tropospheric Emission Spectrometer (TES) and simulated isotope ratios from an isotopically enabled version of the NCAR Community Atmosphere Model (iCAM5), the present study defines isotopic anomalies with respect to a reference water vapor concentration of 4 mmol mol^{-1}. It is shown that this new quantity tracks changes in *E*-*P* that result from large-scale convective reorganization associated with El Niño Southern Oscillation (ENSO). Simulated isotopic anomalies also demonstrate sensitivity to variability in *E*-*P* irrespective of the strength or phase of ENSO at tropical locations outside the Intertropical Convergence Zone. Importantly, the isotopic signal of *E*-*P* in free tropospheric water vapor transfers to the isotope ratios of precipitation. Since precipitation often shapes the isotopic records of proxies used to interpret past climate, the results suggest that multi-decadal observations of both water vapor and precipitation isotope ratios should provide key evidence of shifting regional moisture imbalances now and in the future.

Index terms

Climate dynamics

Convective processes

Global climate models

Precipitation

Remote sensing

Keywords

precipitation, evaporation, divergence, isotope ratio, ENSO, TES

1. Introduction

Although there is a near global balance in evaporation (*E*) and precipitation (*P*), there are regional differences that shape moisture transport globally. Moisture divergence balances these regional differences, so long as changes in moisture storage are negligible:

$$E - P = \nabla \cdot \mathbf{Q}, \qquad (1)$$

where the term on the right hand side is the vertical integral of the moisture flux divergence—with **Q** defined as $\mathbf{V}q$—and is henceforth denoted [DIV] (Fig. 1). Eqn. 1 illustrates why the subtropics, where $E>P$, export moisture to the equator and midlatitudes. As Earth warms, it is predicted that these regional moisture differences will become larger [e.g. *Held and Soden,* 2006]. Consequently, observations that can track E-P are desirable.

Hydrogen isotope ratios in water (e.g. $R = {}^{2}H/{}^{1}H$) are powerful tracers of water cycle processes due to their sensitivity to water phase changes. Because of their lower saturation vapor pressure, heavier isotopes (e.g. ${}^{2}H$ or D) preferentially condense and rain out, while lighter isotopes (e.g. ${}^{1}H$) preferentially evaporate [*Dansgaard*, 1964]. Air masses recently moistened by evaporating surface waters are thus typically characterized by higher isotope ratios than air masses that have recently experienced condensation and precipitation [*Dansgaard*, 196; *Gat*, 1996; *Noone*, 2012]. There is thus reason to expect that isotope ratios track E-P.

Several studies have proposed a relationship between E-P and the isotope ratios of water vapor and precipitation. *Lee et al.* [2007], for example, argued that both water vapor and precipitation will become enriched in heavy isotopes as (*E*-*P*)/*P*—and the relative contribution of local evaporation to precipitation—increases. They found that this relationship explained patterns in an isotopically enabled version of the Community Atmosphere Model version 2 (CAM2) and in precipitation stations throughout the tropics. *Moore et al.* [2014] found a similar relationship in idealized large-eddy simulations of tropical deep convection. Nevertheless, these relationships have yet to be explored in global water vapor datasets from remote-sensing instruments, which provide an opportunity to track variations in *E*-*P* over large geographic regions during both rainy and dry conditions.

This study examines the relationship between the total-column hydrologic balance—represented by the vertically integrated moisture flux divergence [DIV]—and the hydrogen isotope ratio in water vapor estimated from NASA's Tropospheric Emission Spectrometer (TES) over tropical oceanic regions (30°S-30°N). Simulated isotope ratios from NCAR's isotope-enabled Community Atmosphere Model version 5 (iCAM5) are used to examine spatial patterns in a corollary analysis and provide insight where satellite coverage is sparse. As described in the methods, isotopic anomalies are evaluated with respect to a reference water vapor volume mixing ratio (q) of 4 mmol mol^{-1}, rather than a fixed altitude, to assess variations in regional imbalances between evaporation and precipitation. These anomalies are henceforth referred to as δD_q. The analysis suggests reorganization of convective patterns during ENSO (El Niño Southern Oscillation) drives significant spatial variations in both precipitation and moisture flux divergence; however, it is the latter that exerts a particularly strong influence on δD_q. These results suggest δD_q traces *E*-*P* and not precipitation amount alone. Long-term measurements of isotope ratios in water vapor should consequently provide an important signal of changes in the atmospheric hydrological cycle with climate variations.

2. Methods

2.1. Interpreting variations in water isotope ratios

To first order, the hydrogen isotope ratio in water vapor co-varies with the water vapor volume mixing ratio (q), regardless of the moistening or drying processes involved. Figure 2 demonstrates this point by showing the dependence of the isotope ratio (R) on q for two irreversible processes, which span the majority of water isotopic observations globally [*Worden et al.*, 2007; *Lee et al.*, 2011; *Noone*, 2012]. The solid red line shows the isotopic variation of an air mass following Rayleigh distillation [*Dansgaard*, 1964]:

$$R = R_0(q/q_0)^{\alpha-1}, \qquad (2)$$

where 0 represents a reference level (e.g. the lifting condensation level) and α is a temperature-dependent fractionation factor defined by the ratio of saturation vapor pressures for the H_2O and HDO isotopologues. Note that in Fig. 2 and throughout the paper the isotope ratios are expressed in delta notation relative to Vienna Standard Mean Ocean Water (VSMOW): $\delta D=(R/R_{VSMOW}-1)\times1000$. The red curve assumes that an air mass—characterized by $\delta D=-100$ permil, $q=22$ mmol mol^{-1}, and $T=290K$ at the lifting condensation level—rises pseudoadiabatically, so that all water that condenses immediately precipitates. The solid blue line, in contrast, shows the isotopic variation of the same air mass were it instead mixed with the dry free troposphere. Together, these Rayleigh and mixing curves approximate the hydrological cycle: precipitation dehydrates the atmosphere in the tropics (red line) while air masses detrained from deep convective regions and transported downwards by large-scale subsidence are rehydrated by shallow convective mixing (blue line) as they are entrained into cloud-topped boundary layers in the subtropics. Lagrangian analyses have confirmed that these processes tend to deplete and enrich the isotope ratios of air masses, respectively [*Brown et al.*, 2013]. Differences between precipitation- and evaporation-dominated environments are consequently represented by differences in the isotope ratio with respect to q.

2.2. Calculating dD$_q$

To evaluate variations in the isotope ratio with respect to a reference value of q, we define δD_q as the isotope ratio of hydrogen at q=4 mmol mol^{-1}. This quantity is estimated at each point in (horizontal) space and time by regressing the daily mean vertical profile of the HDO volume mixing ratio against the daily mean vertical profile of the H_2O volume mixing ratio and predicting the HDO concentration at 4 mmol mol^{-1}. The HDO concentration is subsequently converted to an isotope ratio and expressed in delta notation. Although atmospheric q is seldom 4 mmol mol^{-1}, it is nevertheless a useful reference humidity since satellite-borne instrumentation is particularly sensitive to isotopic differences between Rayleigh- and mixing-like states (see Fig. 2) at this humidity level [*Bailey*, 2014]. Furthermore, in many locations, it represents a region of the lower free troposphere that explains much of the variance in total column water, which is a strong predictor of deep convective development and precipitation [*Holloway and Neelin*, 2009]. While δD_q bears resemblance to the metric $\Delta\delta D$ used by *Samuels-Crow et al.* [2014]—where $\Delta\delta D$ defines the difference between the isotope ratio estimated from satellite and the isotope ratio predicted from a Rayleigh distillation (Eqn. 2)— δD_q does not require one to make assumptions about the environment near cloud base. Similarities between these metrics are discussed in the Supporting Information.

Observationally based estimates of δD_q are derived from jointly retrieved HDO and H_2O volume mixing ratio (i.e. q) profiles from NASA's Tropospheric Emission Spectrometer (TES) Lite version 6 dataset [*TES*, 2013]. Model-based estimates are derived from daily mean vertical profiles of HDO and H_2O simulated by the isotopically enabled version of NCAR's Community Atmosphere Model version 5 (iCAM5, hereafter simply denoted "CAM") [*Nusbaumer et al.*, 2016]. The model output come from a free-running CAM simulation forced by observed SSTs over the years 1995-2014, with a horizontal resolution of 1.9°N×2.5°E. Although *Nusbaumer et al.* [2016] used the full TES averaging kernel to validate the model's performance, the present study does not adjust the CAM output in this manner. While this decision may limit comparability between the CAM and TES isotopic information presented, it facilitates identification of isotopic variations that may be masked due to the limited vertical resolution of the remote-sensing observations.

TES is an infrared spectrometer that flies aboard the Aura spacecraft as part of NASA's A-Train satellite constellation. The analysis uses retrievals from the nadir-viewing mode, which has a horizontal footprint of 5.3 km×8.3 km. TES Lite products, which are available online from NASA's Atmospheric Science Data Center (https://eosweb.larc.nasa.gov/) [*TES*, 2013], come corrected for known isotopic biases, which are discussed in *Worden et al*. [2011, 2012]. HDO and H_2O volume mixing ratios are provided for seventeen pressure levels; however, the degrees of freedom associated with the HDO profile are typically close to 1. While data coverage spans

Sept. 2004 to the present, spatio-temporal coverage becomes very sparse in the later years. As a result, the analysis focuses on the Sept. 2004 – Dec. 2011 period, which includes the years with greatest global coverage, as well as two El Niño winters (2006-07, 2009-10) and two La Niña winters (2007-08, 2010-11).

Two filters are applied when selecting TES HDO profiles to ensure high quality data. First, only profiles with at least 0.5 degrees of freedom in HDO are selected to ensure that the final retrieval is not excessively biased by a priori assumptions about the true atmospheric state [e.g. *Worden et al.*, 2007; *Noone*, 2012; *Brown et al.*, 2013]. Second, because the sensitivity of the retrieval to the true atmospheric state diminishes while simultaneously shifting upwards as cloudiness increases [*Lee et al.*, 2011], only those retrievals with an average cloud optical depth (COD) less than 3.6 are used. *Lee et al.* [2011] showed that the shape and magnitude of the averaging kernel are comparable for retrievals in clear sky (e.g. COD less than 0.2) and non-precipitating-cloud conditions (e.g. COD greater than 0.2 and less than 3.6). Nevertheless, stricter cloud filters are tested and discussed as part of the analysis. Importantly, since the isotope ratio reflects the integrated condensation history of air masses, isotope ratios measured under non-precipitating conditions still reveal information about precipitation processes occurring close in space and/or time [*Gat et al.*, 1996; *Worden et al.*, 2007; *Brown et al.*, 2008; *Noone*, 2012].

Before the isotope ratio at q=4 mmol mol^{-1} is predicted, the TES HDO and H_2O profiles from each 24-hour period are averaged to a 3°×3° grid matching the gridded product from the ECMWF (European Centre for Medium-Range Weather Forecasts) ERA-Interim reanalysis. Similarly, the daily mean simulated profiles from CAM are interpolated to the ERA grid using nearest neighbor weighting. Daily estimates of δD_q are then calculated for each grid point within the tropical region 30°S-30°N and for the time period Sept. 2004 – Dec. 2011. The top and bottom percentile of TES δD_q are excluded from the analysis to eliminate a small number of outliers whose values lie outside the expected range of lower and mid-tropospheric hydrogen isotope ratios in the Pacific [e.g. *Worden et al.*, 2011; *Bailey et al.*, 2013]. These outliers are the result of poor regression fits between the HDO and H_2O profiles.

2.3. Characterizing changes in **E-P** *with variations in the spatial organization of convection*

Variations in the spatial organization of convection caused by ENSO (El Niño Southern Oscillation) provide a natural test bed for investigating the sensitivity of δD_q to regional moisture imbalances in *E* and *P*. As will be shown in the Results, ENSO phases are also sufficiently long that the equality expressed in Eqn. 1 is satisfied. For the purposes of this study, ENSO differences are estimated by subtracting the average conditions for the two El Niño winters (SONDJF 2006-07 and 2009-10) from the average conditions for the two La Niña winters (SONDJF 2007-08 and 2010-11). Differences in the organization of convection are identified by evaluating variations in daily mean NOAA Interpolated OLR (Outgoing Longwave Radiation, provided by the NOAA/OAR/ESRL PSD, Boulder, Colorado, USA, from their Web site at http://www.esrl.noaa.gov/psd/) [*Liebmann and Smith*, 1996]; daily mean cloud top pressure from TES, filtered and regridded the same as the HDO profiles; daily mean cloud top pressure from the MODIS (Moderate Resolution Imaging Spectroradiometer) version 5 level 3 Aqua dataset (available from https://ladsweb.nascom.nasa.gov/); and MODIS joint histograms of cloud optical depth and cloud top pressure.

The effects of convective reorganization on regional moisture imbalances are characterized by evaluating daily mean *E*, *P*, and [DIV] from ERA-Interim [*Dee et al.*, 2011] and CAM, whose output is interpolated to the ERA 3°×3° grid. Daily mean *E* and *P* from ERA are estimated by summing ECMWF's 12-hour forecast accumulations of evaporation and precipitation, respectively, starting from the 0000 and 1200 UTC time steps. Daily mean [DIV] is estimated by averaging the instantaneous vertical integral of divergence of moisture flux from the 0000, 0600, 1200, and 1800 UTC time steps. In comparison, daily mean [DIV] from CAM is estimated for each grid using finite differences in spherical geometry:

$$[\mathrm{DIV}] = \frac{[uq]_{\lambda+} - [uq]_{\lambda-}}{2(\Delta x \cdot \cos\varphi)} + \frac{[vq]_{\varphi+} - [vq]_{\varphi-}}{2(\Delta y)} \,. \quad (3)$$

The first term differences the vertically integrated zonal moisture flux ([*uq*]) between the grid point to the east and the grid point to the west of the point of interest while the second term differences the vertically integrated meridional moisture flux ([*vq*]) between the grid point to the north and the grid point to the south of the point of interest. Both terms are normalized by the distances over which the differences are calculated. φ and λ are the latitude and longitude in radians, respectively, of the ERA 3°×3° grid points, and Δx and Δy represent the lengths (m) of the two sides of a grid box at the equator.

2.4. Evaluating isotopic changes with variations in **E-P**

To evaluate the sensitivity of isotope ratios to variations in *E*-*P*, the first part of the analysis examines composite differences in daily mean δD_q for distinct patterns of *P*, *E*, and [DIV] associated with ENSO. Composite differences in daily mean δD_z—which is here defined as the δD average for the 800-500-hPa layer of the atmosphere [cf. *Berkelhammer et al.*, 2012; *Sutanto et al.*, 2015]—and the δDs of total column condensate and precipitation in CAM are also examined. While the daily mean δD_z at each grid point is calculated as a mass-weighted average, the composite differences for both TES and CAM are derived from arithmetic temporal means. The δD of total column condensate is estimated for each grid point by vertically integrating the HDO and H_2O concentrations of liquid condensate and ice in CAM and weighting by the depth of each model pressure level.

The second part of the analysis reveals that while spatial variations in [DIV] and *E*-*P* are strongly correlated with spatial variations in *P*, δD_q is more sensitive to measures of column hydrologic balance than to *P* alone. First, composite differences in observed and simulated δD_q are evaluated for periods of high and low [DIV] and *P* irrespective of the strength or phase of ENSO. So-called "high" and "low" periods are defined by the upper and lower quartiles, respectively, of each variable. The quartiles are computed from the daily means for the entire analysis period—Sept. 2004 to Dec. 2011—and for each grid point, to help normalize differences between regions characterized by strong moisture convergence (e.g. the Intertropical Convergence Zone (ITCZ), Fig. 1b) and regions characterized by strong moisture divergence (e.g. the subtropics, Fig. 1b). Second, the composite differences in δD_q for periods of high and low [DIV] are further evaluated for the following narrow precipitation bins: 0-1 mm day^{-1}, 1-2.5 mm day^{-1}, 2.5-5 mm day^{-1}, and 5+ mm day^{-1}. Although the steady-state assumptions of Eqn. 1 are not fully satisfied when assessing daily variability in moisture flux divergence, the spatial dependence of δD_q on [DIV] is sufficiently similar to the spatial dependence of δD_q on *E*-*P* (Pearson correlation coefficient of 0.88) that only the former relationship is discussed in detail in the main text. Readers may refer to the Supporting Information for additional figures showing composite differences of δD_q for periods of high and low *E-P*.

3. Results

3.1. Isotopic variations with large-scale convective reorganization

Between cold (La Niña) and warm (El Niño) phases of ENSO, the hydrological cycle reorganizes significantly. During La Niña, changes in outgoing longwave radiation (OLR; Fig. 3a) indicate deep convection shifts westward, toward Indonesia (box 1, Fig. 3), and convective activity strengthens east of Australia, near Hawaii (box 4, Fig. 3), and off the coasts of Ecuador and Peru (box 5, Fig. 3). In comparison, during El Niño, deep convection shifts toward the central Pacific (boxes 2 and 3, Fig. 3), and convective activity strengthens eastward along the Intertropical Convergence Zone (ITCZ). Composite differences in MODIS cloud top pressure confirm that decreases in OLR are linked to increases in cloud top height, associated with a deepening of the convective column (Fig. 3b). Histograms of cloud top pressure versus cloud optical depth for liquid condensate (Fig. 3d) provide a more detailed picture of the changes in cloudiness with height over the five boxed regions shown in Figs. 3a-c. While west of the dateline strengthening convective activity results in an increase in high clouds, east of the dateline it is mid-level clouds that increase: hence, reductions in OLR are not as great. Importantly, the pattern of these convective changes does not follow sea surface temperature (SST) changes exactly [e.g. *Trenberth and Caron*, 2000], highlighting the importance of dynamical processes in altering moisture transport during El Niño and La Niña.

According to both reanalysis and CAM, changes in precipitation (ERA Fig. 4a; CAM Fig. 5a) broadly follow changes in convective activity and cloud top height as expected. Changes in vertically integrated moisture flux convergence (the negative equivalent of the vertically integrated moisture flux divergence; ERA Fig. 4b; CAM Fig. 5b), are similar in pattern since the loss of atmospheric moisture through precipitation outpaces the increase in evaporative flux (ERA Fig. 4c; CAM Fig. 5c). In essence, transport must maintain the total column moisture necessary to sustain the observed increases in P in the absence of substantive changes in local E. One notable exception to this pattern in the reanalysis is the east Pacific (box 5, Figs. 3-5) where the reanalysis suggests there is no change in P despite the detection of clear decreases in OLR and cloud top pressure by satellite (Fig. 3). Decreases in [DIV] in this region reflect the fact that the balance of E and P shifts even though P remains constant (ERA Fig. 4d; CAM Fig. 5d). Correlations between the ENSO composite difference patterns of [DIV] and E-P exceed 0.97 in both Figs. 4 and 5. A similar spatial pattern of isotopic changes would thus be expected, if the water vapor isotope ratio is indeed a robust metric of column-average hydrologic balance.

To evaluate the sensitivity of the water vapor isotope ratio to variations in E-P, composite differences in δD_z and δD_q with ENSO are examined using both TES observations and CAM output. Although TES retrievals are only selected for periods of low-fractional cloud cover, the retrievals nevertheless discern the large-scale changes in cloud top pressure detected by MODIS (Fig. 3), indicating the satellite spatio-temporal coverage is adequate for investigating broad brush patterns of convective reorganization with ENSO.

As illustrated in Figs. 6a-b and Fig. 7, both TES and CAM show clear changes in δD_z with ENSO; however, these changes are inconsistent with the changes in convective reorganization shown in Fig. 3. West of the dateline (e.g. boxes 1 and 2), isotopic changes are negatively correlated with the precipitation changes brought about by convective reorganization, while in the central Pacific (e.g. box 3), isotopic changes are positively correlated with precipitation. Moreover, TES and CAM disagree in the estimated sign and/or significance of δD_z changes near Hawaii (e.g. box 4) and in the east Pacific (e.g. box 5).

In contrast, changes in δD_q closely follow the changes in convective reorganization with ENSO (Figs. 6c-d; Fig. 7). This is particularly evident in CAM, where decreases in δD_q align with a deepening of convection (see Fig. 3), an increase in P, and a decrease in [DIV]. A similar though noisier pattern is recognizable in the satellite observations, with the exception of the region marked by box 3. There, the TES retrievals suggest δD_q remains constant while CAM predicts δD_q increases. Interestingly, both TES and CAM identify significant changes in δD_q in the east Pacific (box 5, Fig. 7) where [DIV] decreases with E-P but P changes little (e.g. CAM) or not at all (e.g. ERA). This finding supports the hypothesis that δD_q is indeed sensitive to changes in regional moisture imbalances.

Discrepancies between TES and CAM near the dateline—where cloud changes are particularly significant—raise the concern that the satellite observations may be influenced by changes in cloud height and thickness with ENSO [cf. *Lee et al.,* 2011]. This would mean that information provided by satellite-derived water vapor isotope ratios is not in fact independent of information readily available through other measurement systems (e.g. MODIS). Yet this appears not to be the case. Comparing this study's estimates of ENSO changes in δD_z with previous work by *Sutanto et al.* [2015]—whose tolerance for cloudiness was much lower—verifies that the patterns of isotopic change are qualitatively similar. Furthermore, using *Sutanto et al.*'s lower cloud optical depth threshold (0.4) and other quality-control filters to estimate changes in δD_q with ENSO produces a δD_q difference pattern (Fig. S1) that is very similar to the one shown in Fig. 6c. These results suggest that δD_q is an independent metric of changes in convective organization. Discrepancies between TES and CAM may instead be caused by temporal biases in the remotely sensed retrievals or biases in the parameterized representations of CAM's moist physics and/or moisture transport dynamics; however, these hypotheses remain to be tested in future work.

To interpret the information provided by the changes in δD_q with ENSO, we revisit Fig. 2 and the discussion of Section 2.1. The more δD_q decreases, the less hyperbolic and more linear the relationship between the water vapor isotope ratio and volume mixing ratio presumably becomes. This shift from a more hyperbolic (e.g. Fig. 2 "mixing" line) to a more linear (e.g. Fig. 2 "Rayleigh" line) curve on an isotopic diagram is consistent with a transition from a shallow convective environment, in which a temperature inversion separates the boundary layer and free troposphere, to a deeper convective environment, in which the atmosphere is closer in structure to a pseudoadiabat. The variations in δD_q shown in Figs. 6c-d and Fig. 7 are thus not only correlated with but also theoretically consistent with the reorganization in convective activity observed with ENSO. In contrast, δD_z may be influenced by processes with opposing isotopic effects: greater convective activity enriches the lower free troposphere by transporting enriched boundary layer moisture upward [*Sutanto et al.*, 2015] while convergence and precipitation both plausibly act to deplete the atmosphere [e.g. *Dansgaard et al.*, 1964; *Lee et al.*, 2007; *Moore et al.*, 2014]. For these reasons, variations in δD_z may not track changes in large-scale convective activity as unambiguously as variations in δD_q.

It is possible, however, that variations in δD_q could occur without a simultaneous or significant reorganization of convection. For example, one could imagine two environments in which the atmosphere approximates a pseudoadiabat but the boundary layer conditions—and thus cloud base conditions—differ, such as might occur under distinct temperature regimes. Plotting these environments on an isotopic diagram would produce two Rayleigh distillation curves separated in space along the y-axis (compare the dashed and solid red curves in Fig. 2). However, two results suggest variations in δD_q with ENSO are more closely tied to changes in convective reorganization. First, the differences in δD_q for cold and warm phases of ENSO do not follow canonical patterns of SST change [e.g. *Trenberth and Caron*, 2000] as closely as changes in [DIV] and *E-P*. Second, normalizing δD_q by the prediction from a Rayleigh model [cf. *Samuels-Crow et al.*, 2014] largely accounts for differences in boundary layer conditions between ENSO phases (see Supporting Information for a more detailed discussion); yet such normalization does not change the spatial patterns shown in Figs. 6c-d qualitatively (Fig. S2). It thus appears that variations in δD_q with ENSO are reliable indicators of changes in spatial patterns of convective development.

3.2. δD_q sensitivity to **E-P**

Although the east Pacific is one region where simultaneous changes in [DIV] and δD_q occur under ENSO while *P* remains essentially constant, strong spatial coherence in [DIV] and *P* over the vast majority of the tropics makes it difficult to evaluate exactly how sensitive δD_q is to E-P rather than just to P alone. A more thorough evaluation of the sensitivity of δD_q to regional moisture imbalances is thus warranted. To explore the relationship between δD_q and E-P in greater detail, four linear regression models (Table 1) are applied to the CAM composite differences with ENSO. Two models consist of a single predictor variable—the change from La Niña to El Niño in either precipitation (ΔP) or [DIV] (Δ[DIV])—and two models include both of these variables as predictors. Altering the order of the predictors between the multivariate models allows for a closer examination of the effect of multicollinearity.

Three results stand out from Table 1. First, ΔP and Δ[DIV] are both individually significant predictors of the spatial change in δD_q between La Niña and El Niño periods (i.e. $\Delta\delta D_q$); however, the model with Δ[DIV] as the sole predictor has a slightly higher F statistic and a larger r^2, indicating it is more statistically significant and explains more variance. Second, the estimated regression coefficient for Δ[DIV] changes little between the multivariate and univariate models. This finding suggests the correlation between [DIV] and δD_q is not simply a construct of the individual correlations between each of these variables with P. (In contrast, the estimated regression coefficient for ΔP is very sensitive to whether or not a second variable is incorporated in the model.) Third, the regression sum of squares increases, suggesting more variance is explained, when Δ[DIV] is added to the model in which ΔP is used to predict $\Delta\delta D_q$. In contrast, adding ΔP to the model in which Δ[DIV] is the first predictor has no demonstrable impact on the variance explained. Thus, even though changes in precipitation can explain a large part of the isotopic variability related to shifting hydrological imbalances brought about by convective reorganization with ENSO, a measure of the column-average hydrologic balance—such as [DIV] or *E*-*P*—serves as a more robust predictor of changes in δD_q. Consequently, δD_q emerges as a robust proxy for E-P.

If the variations in δD_q with ENSO are not simply correlated with but caused by shifting regional moisture imbalances, we can hypothesize 1) that δD_q should covary with [DIV] (or *E*-*P*) irrespective of the strength or phase of ENSO and 2) that these relationships should exist even if *P* remains constant. To test these suppositions, composite differences in δD_q are computed for periods of high and low [DIV] and periods of high and low *P* at each grid point for the entire Sept. 2004 – Dec. 2011 period (refer to Section 2.4 for a complete description of the methods). Equivalent composite differences for periods of high and low *E*-*P* are provided for reference in the Supporting Information to show that the steady-state assumption of Eqn. 1 is still reasonable despite the shorter timescale of variability considered. As shown in Fig. 8, CAM δD_q decreases at most grid points as [DIV] decreases and *P* increases (Figs. 8a-b), supporting the idea that δD_q is sensitive to changing convective activity even on daily timescales. Moreover, δD_q responds more consistently to changes in [DIV] than to changes in *P*. There are, nevertheless, a number of regions in which CAM δD_q shows little sensitivity to either variable. For example, in the subtropical stratocumulus regions and parts of the east Pacific equatorial zone, low sensitivity in CAM δD_q may reflect the fact that the modeled [DIV] and *P* vary little on average at these locations. The reason for the lack of sensitivity in the west Pacific equatorial zone is less clear but is revisited in Section 4.

Composite differences in TES δD_q (Figs. 8c-d), in comparison, show much weaker sensitivity, possibly reflecting both limited temporal coverage and instrumental and retrieval uncertainties in the remotely sensed data product. One key consideration, for example, is that because TES retrievals near raining clouds are excluded from the analysis, the high *P* and low [DIV] composites must be comprised of observations taken in low-fractional cloud cover pockets in which *P* and [DIV] likely differ from the grid-averaged conditions. This becomes more critical a concern when assessing daily variations in convective activity as compared to long duration changes associated with large-scale climate variability. Nevertheless, several conclusions may be drawn: 1) similar to CAM, TES δD_q decreases more consistently with decreasing [DIV] than with increasing *P*; 2) unlike CAM, TES δD_q correlates with [DIV] in the west Pacific equatorial zone; and 3) TES δD_q noticeably anticorrelates with [DIV] in the east Pacific equatorial zone. Interestingly, convergence along the east Pacific Intertropical Convergence Zone (ITCZ) tends to occur low in the atmosphere [*Back and Bretherton*, 2006] and is strongly linked to SST gradients [*Back and Bretherton*, 2009]. One possibility warranting future study is that increasing SSTs associated with decreasing [DIV] have a sufficiently strong enriching effect on the isotope ratios of the boundary layer (see Fig. 2, for example) to reverse the relationship between δD_q and [DIV] in this region.

To further test the sensitivity of δD_q to shifting regional moisture imbalances, we evaluate the response of δD_q to [DIV] independent of *P* by plotting composite differences in CAM δD_q for the upper and lower quartiles of [DIV] associated with narrow precipitation bins at each grid location (Fig. 9). Scatter plots (not shown) confirm that binning eliminates the co-dependence of [DIV] and *P*, except for the highest precipitation bin (e.g. 5+ mm day^{-1}). As before, equivalent composite differences in CAM δD_q for the upper and lower quartiles of *E*-*P* are provided for reference in the Supporting Information. For all precipitation bins, CAM shows broad correlations between δD_q and [DIV], consistent with the hypothesis that δD_q does indeed track *E*-*P* and not *P* alone. However, the equatorial region is once again an exception to this pattern (note the recognizable double ITCZ structure in the area characterized by weak δD_q response). δD_q is thus not an unambiguous tracer of daily variability in *E*-*P* everywhere. Still, extensive regions of the subtropics appear ideal for monitoring changes in regional moisture imbalances even in the absence of convective reorganization associated with large-scale climate variability.

4. Summary and Discussion

This study develops a new metric—δD_q—to characterize isotopic anomalies in the water vapor isotope ratio with respect to a reference water vapor volume mixing ratio of 4 mmol mol^{-1}. Composite differences in δD_q between cold and warm phases of ENSO are estimated using both remotely sensed observations from the Tropospheric Emission Spectrometer (TES) and simulations from the Community Atmosphere Model (CAM). The analysis shows that δD_q tracks regional moisture imbalances between evaporation and precipitation—represented by changes in [DIV]—when large-scale reorganization of convection takes place, even if the amount of precipitation changes little or not at all. The analysis further uses composite differences between periods of high and low [DIV] to show that δD_q tracks variations in *E*-*P* irrespective of the phase or strength of ENSO in tropical regions outside the Intertropical Convergence Zone (ITCZ).

The results corroborate modeling studies by *Lee et al.* [2007] and *Moore et al.* [2014], which previously argued that the isotope ratio of water vapor—and therefore the precipitation that forms from it—decreases as moisture convergence increases to sustain higher precipitation rates (e.g. $P>E$). Figure 10 provides additional evidence for this hypothesis by showing composite differences in the isotopic composition of CAM total column condensate and precipitation for distinct phases of ENSO. Both variables mirror the δD_q composite differences between La Niña and El Niño periods shown earlier (Fig. 6d), indicating that cloud and precipitation isotopic changes are also spatially correlated with the variations in regional moisture imbalances that result from large-scale convective reorganization. With precipitation isotopic measurements from the Global Network of Isotopes in Precipitation (GNIP) dating back to the 1950s, Fig. 10 suggests it should be possible to investigate changes in convective activity over a much longer time span than the satellite record, albeit at a significantly reduced number of locations.

Together these studies support a growing body of work that suggests isotopic information in modern and paleo-precipitation records can be used to interpret changes in the organization of regional convective activity [*Cobb et al.*, 2007; *Kurita et al.*, 2009; *Kurita*, 2013; *Moerman et al.*, 2013; *Lekshmy et al.*, 2014; *Samuels-Crow et al.*, 2014; *Sutanto et al.*, 2015; *Aggarwal et al.,* 2016]. This viewpoint differs from a more traditional interpretation of precipitation isotope ratios as indicators of variations in local precipitation intensity or amount [e.g. *Dansgaard,* 1964; *Cruz et al.*, 2005; *Tierney et al.,* 2008; *Niedermeyer et al.*, 2010; *Sano et al.*, 2012]. Although appearing frequently in the literature, the latter has proven problematic since the exact relationship between local precipitation isotope ratios and amount varies widely across tropical locations [*Kurita*, 2013; *Lekshmy et al.*, 2014]. It is also statistically insignificant at many sites on time scales shorter than one month [*Kurita et al.*, 2009; *Conroy et al.*, 2016]—a puzzling finding given that both precipitation rate and isotope ratios vary dramatically over the lifetime of individual storms [*Coplen et al.*, 2008; *Good et al.*, 2014]. As this study shows, changes in regional moisture imbalances with increasing convective activity—represented by decreases in

E-*P* and [DIV]—explain water isotopic variations even in the absence of significant changes in precipitation.

Although it is convenient to think of *E*-*P* as representing a balance between isotopically enriching and depleting processes as discussed in Section 2.1, in actuality the moisture transport required to sustain precipitation may be a critical mechanism by which the isotope ratios of water vapor and precipitation are reduced. To explain why convergence has such a strong influence on water isotope ratios, *Moore et al.* [2014] invoked the fact that the isotope ratio of the atmosphere tends to decrease with height in the lower and mid-troposphere. Consequently, when convection intensifies and the layer of convergence deepens, the moisture entrained into the convective column is more depleted. While the connection between well-organized convection and strong mid-level inflow is well established [*Houze*, 2004], only recently has new work confirmed that the isotope ratio of precipitation decreases when the mean level of convergence increases, even if the precipitation rate remains constant [*Torri et al.*, 2016].

These arguments not only provide a mechanistic explanation for the broad geographic correlations found between [DIV] and δD_q, but they also possibly elucidate the unexpected increases in δD_q observed with decreasing [DIV] near the ITCZ in Fig. 9. One could imagine, for instance, that if the mean level of moisture entrained decreased while total column convergence increased, then the isotope ratio of water vapor in the convective column could increase, contrary to expectation. Interestingly, the unexpected increases in δD_q with decreasing [DIV] are somewhat stronger in the central and east Pacific, where “bottom-heavy” vertical velocity profiles maintain a low mean level of moisture entrainment even when convection intensifies [*Back and Bretherton*, 2006; *Torri et al.*, 2016].

Of course, other factors could also contribute to the ambiguous relationship between daily variations in δD_q and [DIV] near the equator. *Feng et al.* [2009], for instance, argued that while there are strong correlations between seasonal trends in precipitation isotope ratios and [DIV], a slight lag in the correlation indicates that evaporative enrichment plays a nontrivial role. This may be particularly true if steady-state assumptions are violated, and changes in moisture storage are nontrivial, which is more likely to be the case for the quartile differences in daily [DIV] plotted in Figs. 8-9 than the seasonal composite differences plotted in Figs. 4-5. Others have argued that post-condensational processes, such as rain re-evaporation, significantly influence the water vapor and precipitation isotope ratios in convection [e.g. *Risi et al.*, 2008; *Wright et al.*, 2009; *Kurita*, 2013]. These microphysical processes could obfuscate correlations between δD_q and moisture transport on shorter timescales. Similarly, large-scale advection could shift the isotopic trace of convection to areas "downstream" [e.g. *Gedzelman*, 1988; *Galewsky et al.*, 2007; *Bailey et al.*, 2013], reducing the correlation between δD_q and [DIV] at a particular location.

Given the myriad processes that influence the isotopic composition of water vapor [*Galewsky et al.*, 2016], it is unlikely that [DIV] is the sole predictor of daily isotopic variations at a particular location. However, this study demonstrates that longer duration shifts in regional moisture imbalances do leave a significant and observable imprint on the isotope ratio of water vapor, and, consequently, the isotope ratios of precipitation, which influence the paleoproxy record. These results indicate that water isotope ratios can provide independent verification of variations in *E*-*P* in both the past and present.

Key to identifying this signal is the new metric δD_q, which is much more sensitive than the isotope ratio at a fixed altitude to changes in [DIV] and *E*-*P*. This difference in sensitivity, initially revealed by Fig. 6, is further demonstrated by comparing Fig. 11 with Fig. 9c. While δD_q shows some sensitivity to daily variations in [DIV] at most locations outside the ITCZ, δD_z shows very little. The reason for this difference may be understood by considering an environment dominated by a single process, such as evaporative mixing. As the blue line in Fig. 2 shows, variations in specific humidity can cause isotopic variations large enough that they easily dwarf variations associated with a shift in hydrological process. By normalizing the isotope ratio with respect to water vapor concentration, δD_q isolates the portion of isotopic variability most closely associated with the shift from evaporation- to precipitation-dominated regimes and vice versa. Since this new metric can be derived from remote-sensing observations, near-global changes in regional moisture imbalances can be monitored.

By extension, these results suggest that isotope ratios in water vapor and precipitation should serve as powerful tracers of future climate variability—an important finding given the difficulty of measuring both evaporation and precipitation globally. As climate warms, regional differences in evaporation and precipitation are likely to become more disparate, causing the drier *E*-dominated regions of the tropics to become drier and the wetter *P*-dominated regions to become wetter [*Held and Soden*, 2006]. Satellite observations of recent changes in tropical precipitation support these predictions [*John et al.*, 2009; *Allan et al.*, 2010; *Li et al.*, 2011; *Zhou et al.*, 2011], as do in situ measurements of changes in ocean salinity [*Helm et al.*, 2010; *Durack et al.*, 2012]. The growing disparity in *E-P* regionally is expected to drive greater horizontal moisture divergence [*Held and Soden*, 2006], widening the distance between moisture sources and sinks and increasing the residence time of moisture in the atmosphere [*Singh et al.*, 2016]. This prediction is supported by observed decreases in precipitation relative to total column water in tropical regions north and south of the ITCZ [*Li et al.*, 2011]. Previous research has already shown that precipitation isotope ratios are significantly correlated with the residence time of moisture in the atmosphere [*Aggarwal et al.*, 2012]. This study's findings suggest variations in *E-P* are what underpins these relationships and provide evidence that long-term measurements of water vapor and precipitation isotope ratios can be used to monitor key hydrological trends with climate.

Acknowledgements

A. Bailey thanks the Joint Institute for the Study of the Atmosphere and Ocean for a postdoctoral research fellowship that supported this research, as well as H. Singh at the University of Washington for numerous thought-provoking discussions on hydroclimate variability. P. Blossey and D. Noone were supported by the NASA Modeling, Analysis and Prediction Program through grant number NNX13AN47G. J. Nusbaumer and the development of the isotopic version of CAM were supported by the NSF Paleoclimate program (AGS-1049104) and Climate and Large Scale Dynamics program as part of a Faculty Early Career Development award (AGS-0955841), and made use of computing resources provided by the Climate Simulation Laboratory at the National Center for Atmospheric Research's Computational and Information Systems Laboratory, sponsored by the National Science Foundation. Data used in this analysis may be located via the references and websites cited in the main text.

References

Aggarwal, P. K., U. Romatschke, L. Araguas-Araguas, D. Belachew, F. J. Longstaffe, P. Berg, C. Schumacher, and A. Funk (2016), Proportions of convective and stratiform precipitation revealed in water isotope ratios, *Nature Geosci.*, *9*, 624-629, doi:10.1038/ngeo2739.

Aggarwal, P. K., O. A. Alduchov, K. O. Froehlich, L. J. Araguas-Araguas, N. C. Sturchio, and N. Kurita (2012), Stable isotopes in global precipitation: A unified interpretation based on atmospheric moisture residence time, *Geophys. Res. Lett.*, *39*, L11705, doi:10.1029/2012GL051937.

Allan, R. P., B. J. Soden, V. O. John, W. Ingram, and P. Good (2010), Current changes in tropical precipitation, *Environ. Res. Lett.*, *5*, 025205, doi:10.1088/1748-9326/5/2/025205.

Back, L. E., and C. S. Bretherton (2006), Geographic variability in the export of moist static energy and vertical motion profiles in the tropical Pacific, *Geophys. Res. Lett.*, *33*, L17810, doi:10.1029/2006GL026672.

Back, L. E., and C. S. Bretherton (2009), On the relationship between SST gradients, boundary layer winds, and convergence over the tropical oceans , *J. Climate*, *22*, 4182-4196, doi:http://dx.doi.org/10.1175/2009JCLI2392.1.

Bailey, A., D. Toohey, and D. Noone (2013), Characterizing moisture exchange between the Hawaiian convective boundary layer and free troposphere using stable isotopes in water, *J. Geophys. Res.*, *118*, 8208-8221, doi:10.1002/jgrd.50639.

Bailey, A. (2014), Evaluating shallow convective mixing and precipitation processes using isotope ratios in water vapor, Ph.D. thesis, Dep. of Atmos. Ocean. Sci., Univ. of Colorado Boulder, Boulder, Colorado, USA.

Berkelhammer, M., C. Risi, N. Kurita, and D. Noone (2012), The moisture source sequence for the Madden-Julian Oscillation as derived from satellite retrievals of HDO and H_2O, *J. Geophys. Res.*, *117*, D03106, doi:10.1029/2011JD016803.

Brown, D., J. Worden, and D. Noone (2008), Comparison of atmospheric hydrology over convective continental regions using water vapor isotope measurements from space, *J. Geophys. Res.*, *113*, D15124, doi:10.1029/2007JD009676.

Brown, D., J. Worden, and D. Noone (2013), Characteristics of tropical and subtropical atmospheric moistening derived from Lagrangian mass balance constrained by measurements of HDO and H2O, *J. Geophys. Res.*, *118*, 54-72, doi:10.1029/2012JD018507.

Cobb, K., M., J. F. Adkins, J. W. Partin, and B. Clark (2007), Regional-scale climate influences on temporal variations of rainwater and cave dripwater oxygen isotopes in northern Borneo, *Earth. Planet. Sci. Lett.*, *263*, 207-220, doi:10.1016/j.epsl.2007.08.024.

Conroy, J. L., D. Noone, K. M. Cobb, J. W. Moerman, and B. L. Konecky (2016), Paired stable isotopologues in precipitation and vapor: A case study within western tropical Pacific storms, *J. Geophys. Res.*, *121*, 3290-3303, doi:10.1002/2015JD023844.

Coplen, T. B., P. J. Neiman, A. B. White, J. M. Landwehr, F. M. Ralph, M. D. Dettinger (2008), Extreme changes in the stable hydrogen isotopes and precipitation characteristics in a landfalling Pacific storm, *Geophys. Res. Lett.*, *21*, L21808, doi:10.1029/2008GL035481.

Cruz, Jr., F. W., S. J. Burns, I. Karmann, W. D. Sharp, M. Vuille, A. O. Cardoso, J. A. Ferrari, P. L. Silva Dias, and O. Viana, Jr. (2005), Insolation-driven changes in atmospheric circulation over the past 116,000 years in subtropical Brazil, *Nature*, *434*, 63-66, doi:10.1038/nature03365.

Dansgaard, W. (1964), Stable isotopes in precipitation, *Tellus*, *16*, 436-468.

Dee, D. P., S. M. Uppala, A. J. Simmons, P. Berrisford, P. Poli, S. Kobayashi, U. Andrae, M. A. Balmaseda, G. Balsamo, P. Bauer, P. Bechtold, A. C. M. Beljaars, L. van de Berg, J. Bidlot, N. Bormann, C. Delsol, R. Dragani, M. Fuentes, A. J. Geer, L. Haimberger, S. B. Healy, H. Hersbach, E. V. Hólm, L. Isaksen, P. Kållberg, M. Köhler, M. Matricardi, A. P. McNally, B. M. Monge-Sanz, J.-J. Morcrette, B,-K. Park, C. Peubey, P. de Rosnay, C. Tavolato, J.-N. Thépaut, F. and Vitart (2011), The ERA-Interim reanalysis: configuration and performance of the data assimilation system, *Q.J.R. Meteorol. Soc.*, *137,* 553–597, doi:10.1002/qj.828.

Durack, P. J. S. E. Wijffels, and R. J. Matear (2012), Ocean salinities reveal strong global water cycle intensification during 1950 to 2000, *Science*, *336*, 455-458, doi:10:1126/science.1212222.

Feng, X., A. M. Faiia, and E. S. Posmentier (2009), Seasonality of isotopes in precipitation: A global perspective, *J. Geophys. Res.*, *115*, D08116, doi:10.1029/2008JD011279.

Galewsky, J., M. Strong, and Z. D. Sharp (2007), Measurements of water vapor D/H ratios from Mauna Kea, Hawaii, and implications for subtropical humidity dynamics, *Geophys. Res. Lett.*, 34, L22808, doi:10.1029/2007GL031330.

Galewsky, J., H. C. Steen-Larsen, R. D. Field, J. Worden, C. Risi, and M. Schneider (2016), Stable isotopes in atmospheric water vapor and applications to the hydrologic cycle, *Rev. Geophys.*, doi:10.1002/2015RG000512.

Gat, J. R. (1996), Oxygen and hydrogen isotopes in the hydrologic cycle, *Annu. Rev. Earth Planet. Sci.*, *24* 225-262.

Gedzelman, S. D. (1988), Deuterium in water vapor above the atmospheric boundary layer, *Tellus*, *40B*, 134-147.

Good, S. P., D. V. Mallia, J. C. Lin, and G. J. Bowen (2014), Stable isotope analysis of precipitation samples obtained via crowdsourcing reveals the spatiotemporal evolution of Superstorm Sandy, *PLoS ONE*, *9*, e91117, doi:10.1371/journal.pone.0091117.

Held I. M., and B. J. Soden (2006), Robust responses of the hydrological cycle to global warming, *J. Climate*, *19*, 5686-5699.

Helm, K. P., N. L. Bindoff, and J. A. Church (2010), Changes in the global hydrological-cycle inferred from ocean salinity, *Geophys. Res. Lett.*, 37, L18701, doi:10.1029/2010GL044222.

Holloway, C. E., and J. D. Neelin (2009), Moisture vertical structure, column water vapor, and tropical deep convection, *J. Atmos. Sci.*, *66*, 1665-1683, doi:10.1175/2008JAS2806.1.

Houze, R. A. Jr. (2004), Mesoscale convective systems, *Rev. Geophys.*, *42*, RG4003, doi:10.1029/2004RG000150.

John, V. O., R. P. Allan, and B. J. Soden (2009), How robust are observed and simulated precipitation responses to tropical ocean warming?, *Geophys. Res. Lett.*, *36*, L14702, doi:10.1029/2009GL038276.

Kurita, N. (2013), Water isotopic variability in response to mesoscale convective system over the tropical ocean*, J. Geophys. Res. Atmos.*, *118*, 10,376–10,390, doi:10.1002/jgrd.50754.

Kurita, N.*,* K. Ichiyanagi*,* J. Matsumoto*,* M. D. Yamanaka, and T. Ohata (2009), The relationship between the isotopic content of precipitation and the precipitation amount in tropical regions, *J. Geochem. Explor.*, *102*, 113–122, doi:10.1016/j.gexplo.2009.03.002.

Lee, J., J. Worden, D. Noone, K. Bowman, A. Eldering, A. LeGrande, J.-L. F. Li, G. Schmidt, and H. Sodemann (2011), Relating tropical ocean clouds to moist processes using water vapor isotope measurements, *Atmos. Chem. Phys.*, *11*, 741-752, doi:10.5194/acp-11-741-2011.

Lee, J.-E., I. Fung, D. J. DePaolo, and C. C. Henning (2007), Analysis of the global distribution of water isotopes using the NCAR atmospheric general circulation model, *J. Geophys. Res.*, *112*, D16306, doi:10.1029/2006JD007657.

Lekshmy, P. R., M. Midhun, R. Ramesh, and R. A. Jani (2014), ^{18}O depletion in monsoon rain relates to large scale organized convection rather than the amount of rainfall, *Scientific Reports*, *4*, doi:10.1038/srep05661.

Li, L., X. Jiang, M. T. Chahine, E. T. Olsen, E. J. Fetzer, L. Chen, and Y. L. Yung (2011), The recycling rate of atmospheric moisture over the past two decades (1988-2009), *Environ. Res. Lett.*, *6*, 034018, doi:10.1088/1748-9326/6/3/034018.

Liebman, B., and C. A. Smith (1996), Description of a complete (interpolated) Outgoitn Longwave Radiation dataset, *Bull. Am. Meteorol. Soc.*, *77*, 1275-1277.

Moerman, J. W., K. M. Cobb, J. F. Adkins, H. Sodemann, B. Clark, and A. A. Tuen (2013), Diurnal to interannual rainfall δ^{18}O variations in northern Borneo driven by regional hydrology, *Earth Planet. Sci. Lett.*, *369-370*, 108-119, doi:10.1016/j.epsl.2013.03.014.

Moore, M*.,* Z. Kuang*, and* P. N. Blossey *(*2014*),* A moisture budget perspective of the amount effect*, Geophys. Res. Lett., 41,* 1329–1335*, doi:10.1002/2013GL058302.*

Niedermeyer, E. M., E. Schefuß, A. L. Sessions, S. Mulitza, G. Mollenhauer, M. Schulz, and G. Wefer (2010), Orbital- and millennial-scale changes in the hydrologic cycle and vegetation in the western African Sahel: insights from individual plant wax δD and δ^{13}C, *Quat. Sci. Rev.*, *29*, 2996-3005, doi:10.1016/j.quascirev.2010.06.039.

Noone, D. (2012), Pairing measurements of the water vapor isotope ratio with humidity to deduce atmospheric moistening and dehydration in the tropical midtroposphere, *J. Climate*, *25*, 4476–4494.

Nusbaumer, J., Wong, T., Bardeen, C., and D. Noone (2016), Evaluating hydrological processes in the Community Atmosphere Model Version 5 (CAM5) using stable isotope ratios of water, *J. Adv. Model Earth Syst.*, *in prep*.

Risi, C., S. Bony, and F. Vimeux (2008), Influence of convective processes on the isotopic composition (δ^{18}O and δD) of precipitation and water vapor in the tropics: 2. Physical interpretation of the amount effect, *J. Geophys. Res.*, *113*, D19306, doi:10.1029/2008JD009943.

Samuels-Crow, K. E., J. Galewsky, D. R. Hardy, Z. D. Sharp, J. Worden, and C. Braun (2014), Upwind convective influences on the isotopic copoisition of atmospheric water vapor over the tropical Andes, *J. Geophys. Res.*, *119*, 7051-7063, doi:10.1002/2014JD021487.

Sano, M., C. Xu, T. Nakatsuka (2012), A 300-year Vietnam hydroclimate and ENSO variability record reconstructed from tree ring δ^{18}O, *J. Geophys. Res.*, *117*, D12115, doi:10.1029/2012JD017749.

Singh, H., C. Bitz, A. Donohoe, J. Nusbaumer, and D. Noone (2016), A mathematical framework for analysis of water Tracers: Part II, understanding large-scale perturbations in the hydrological cycle due to CO_2-doubling, *J. Climate*, doi:10.1175/JCLI-D-16-0293.1, in press.

Sutanto, S. J., G. Hoffmann, J. Worden, R. A. Scheepmaker, I. Aben, and T. Röckmann (2015), Atmospheric processes governing the changes in water isotopologues during ENSO events from model and satellite measurements, *J. Geophys. Res.*, *13*, 6712-6729, doi:10.1002/2015JD023228.

TES Science Team (2013), TES/Aura Level 2, HDO Limb, version 6, Hampton, VA, USA: NASA Atmospheric Science Data Center (ASDC), Accessed TES/Aura L2 Deuterium Oxide (HDO) Lite Nadir (TL2HDOLN) data at doi:10.5067/AURA/TES/TL2HDOLN_L2.006.

Tierney, J. E., J. M. Russell, Y. Huang, J. S. Sinninghe Damsté, E. C. Hopmans, and A. S. Cohen (2008), Northern Hemisphere controls on tropical southeast African climate curing the past 60,000 years, *Science*, *322*, 252-255, doi:10.1126/science.1160485.

Torri, G., D. Ma, and Z. Kuang (2016), Stable water isotopes and large-scale vertical motions in the tropics, *J. Climate*, *in review*.

Trenberth, K. E., and J. M. Caron (2000), The Southern Oscillation revisited: Sea level pressures, surface temperatures, and precipitation, *J. Climate*, *13*, 4358-4365, doi:http://dx.doi.org/10.1175/1520-0442(2000)013<4358:TSORSL>2.0.CO;2.

Worden, J., D. Noone, K. Bowman, and The Tropospheric Emission Spectrometer science team and data contributors (2007), Importance of rain evaporation and continental convection in the tropical water cycle, *Nature*, *445*, 528-532, doi:10.1038/nature05508.

Worden, J., D. Noone, J. Galewsky, A. Bailey, K. Bowman, D. Brown, J. Hurley, S. Kulawik, J. Lee, and M. Strong (2011), Estimate of bias in Aura TES HDO/H_2O profiles from comparison of TES and in situ HDO/H_2O measurements at the Mauna Loa observatory, *Atmos. Chem. Phys.*, *11*, 4491-4503, doi:10.5194/acp-11-4491-2011.

Worden, J., S. Kulawik, C. Frankenberg, V. Payne, K. Bowman, K. Cady-Peirara, K. Wecht, J.-E. Lee, and D. Noone (2012), Profiles of CH_4, HDO, H_2O, and N_2O with improved lower tropospheric vertical resolution from Aura TES radiances, *Atmos. Meas. Tech.*, *5*, 397–411, doi:10.5194/amt-5-397-2012.

Wright, J. S., A. H. Sobel, and G. A. Schmidt (2009), Influence of condensate evaporation on water vapor and its stable isotopes in a GCM, *Geophys. Res. Lett.*, *36*, L12804, doi:10.1029/2009GL038091.

Zhou, Y. P., K.-M. Xu, Y. C. Sud, and A. K. Betts (2011), Recent trends of the tropical hydrological cycle inferred from Global Precipitation Climatology Project and International Satellite Cloud Climatology Project data, *J. Geophys. Res.*, *116*, D09101, doi:10.1029/2010JD015197.

Tables

Table 1. Coefficients, sequential regression sums of squares (SS; expressed relative to the total sum of squares), r^2 values, and F statistics for four linear regression models predicting the change in CAM δD_q with ENSO ($\Delta\delta D_q$).

Model	***a***	***b***	***c***	$\mathbf{SS}_{\Delta P}$	$\mathbf{SS}_{\Delta[\mathrm{DIV}]}$	$\boldsymbol{r^2}$	***F***
$a+b\Delta P$	-0.99 (0.22)	-4.70 (0.13)	---	0.35	---	0.35	1248
$a+c\Delta[\mathrm{DIV}]$	-0.73 (0.22)	---	4.55 (0.12)	---	0.39	0.39	1465
$a+b\Delta P+c\Delta[\mathrm{DIV}]$	-0.77 (0.21)	-0.75* (0.35)	3.91 (0.32)	0.35	0.04	0.39	736.1
$a+c\Delta[\mathrm{DIV}]+b\Delta P$		same as above		0.39	0.00	0.39	736.1

ΔP is the change in CAM precipitation with ENSO, and Δ [DIV] is the change in CAM vertically integrated moisture flux divergence with ENSO. All coefficients and F statistics are characterized by $p<0.001$ except for the coefficient marked by the *, which has $0.05>p>0.01$. The standard error associated with each coefficient estimate is shown in parentheses.

Figures

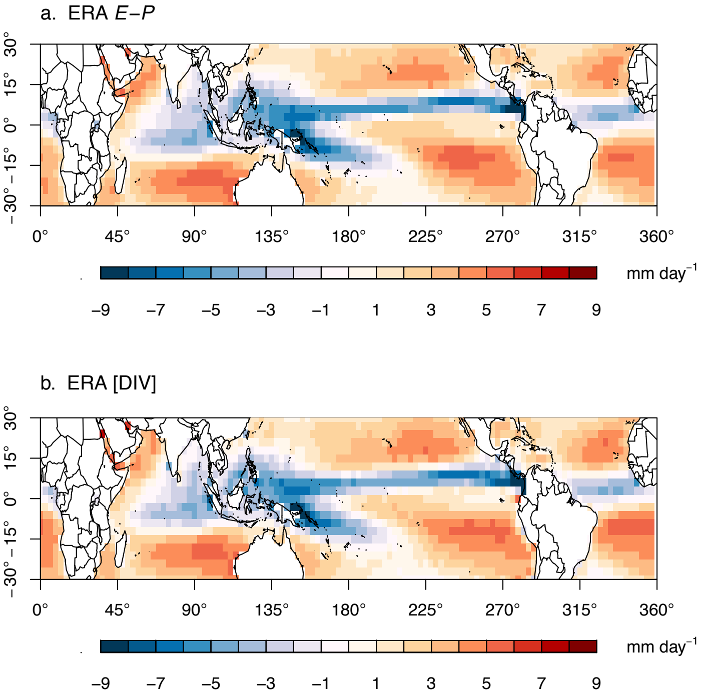

Figure 1. Mean patterns of (a) E-P and (b) [DIV] derived from daily mean estimates of these variables from the ERA-Interim reanalysis for the period Sept. 2004 – Dec. 2011.

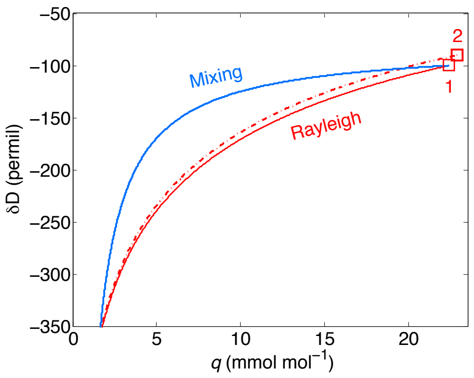

Figure 2. An isotopic diagram showing hypothetical variations in the isotope ratio δD as a function of the water vapor volume mixing ratio q. Box 1 (δD = -100 permil, q = 22 mmol mol^{-1} and T = 290K at the lifting condensation level) shows the departure point for two processes: Rayleigh distillation of an air mass (red line) and mixing between that air parcel and a hypothetical free tropospheric air mass with δD=-400 permil and q=1.4 mmol mol^{-1} (solid blue curve). The dashed red line represents a Rayleigh distillation process for an air mass hypothetically originating from a region of warmer SST (Box 2, δD=-90 permil and q=23 mmol mol^{-1} at a lifting condensation level defined by T=290K).

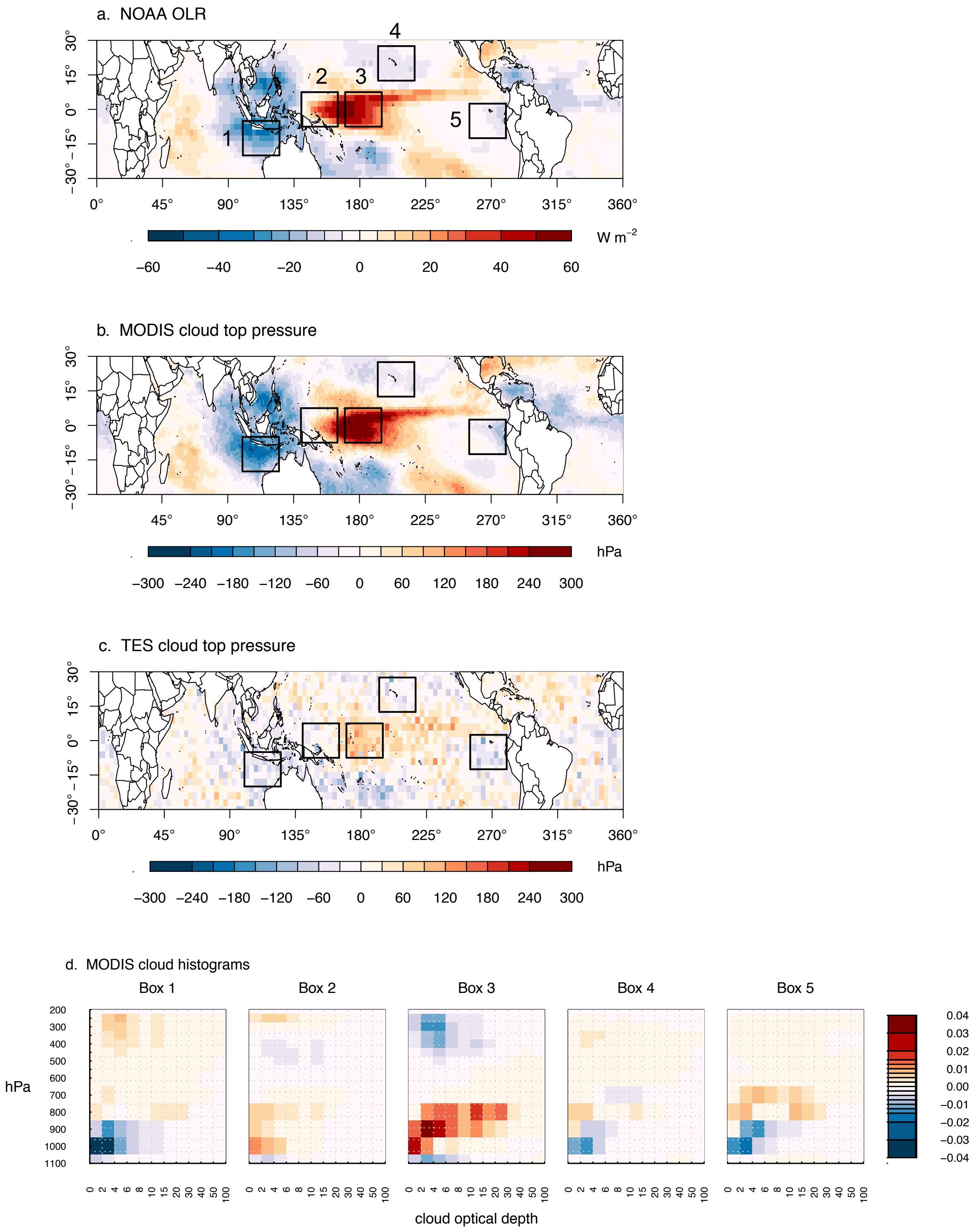

Figure 3. Changes in convective organization with ENSO. Composite differences in (a) NOAA OLR, (b) MODIS cloud top pressure, and (c) TES cloud top pressure for cold minus warm

phases of ENSO. NOAA OLR and MODIS cloud top pressure are plotted on their native 2.5°×2.5° and 1°×1° grids, respectively. (d) Composite differences in the MODIS joint histograms of cloud top pressure and cloud optical depth with ENSO are also shown for liquid cloud for the five boxed regions labeled in panel (a).

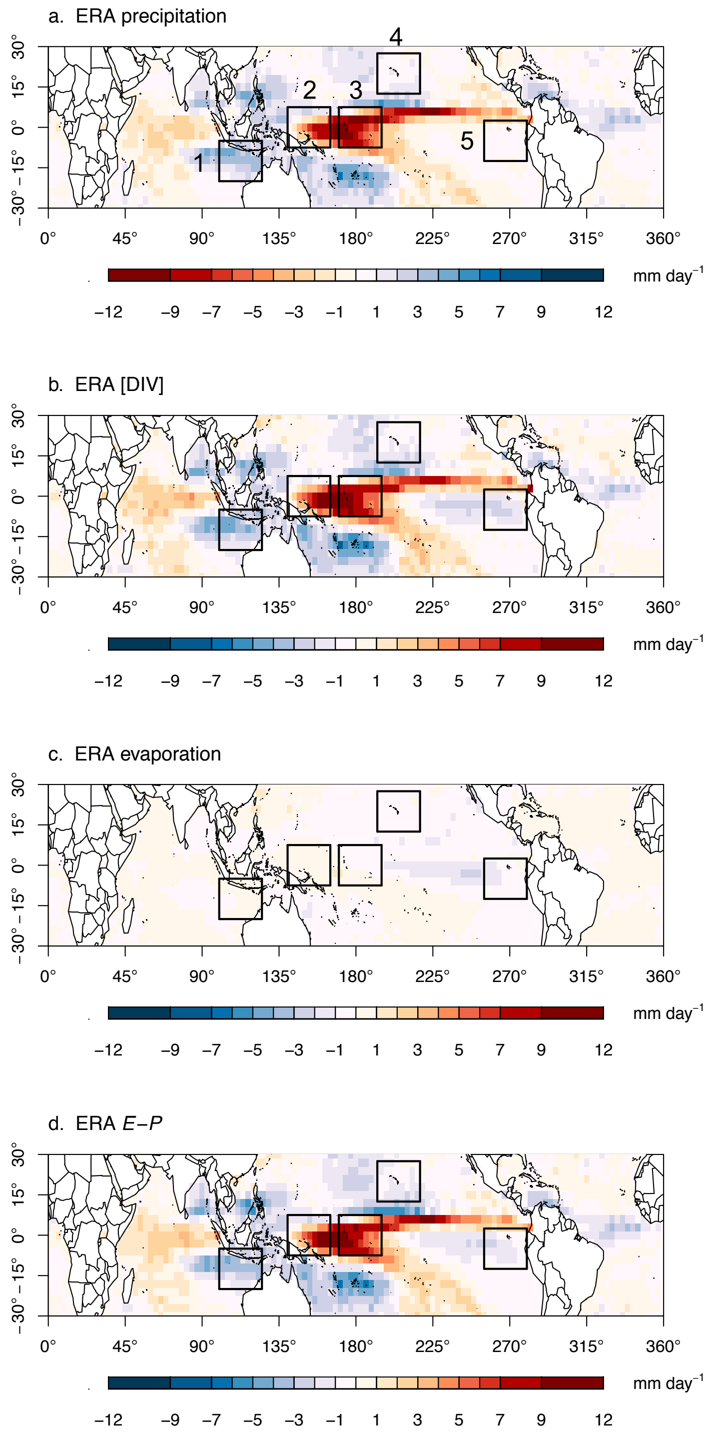

Figure 4. Changes in hydrologic balance with ENSO. Composite differences in (a) ERA precipitation, (b) ERA [DIV], (c) ERA evaporation, and (d) ERA *E*-*P* for cold minus warm phases of ENSO.

a. CAM precipitation

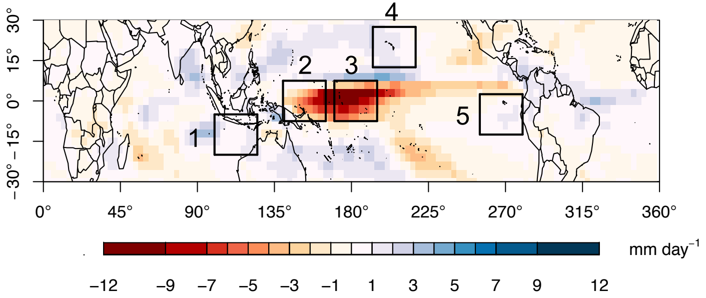

b. CAM [DIV]

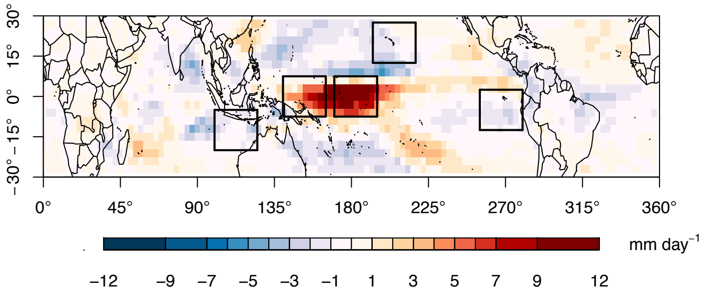

c. CAM evaporation

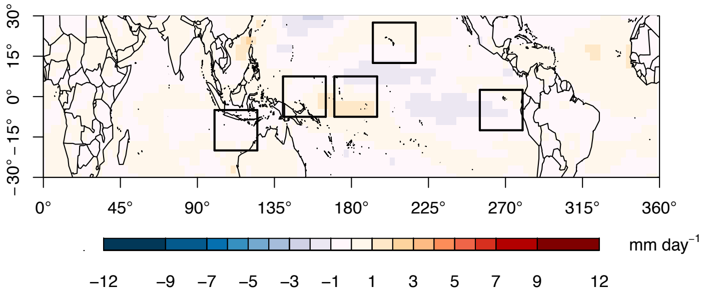

d. CAM *E−P*

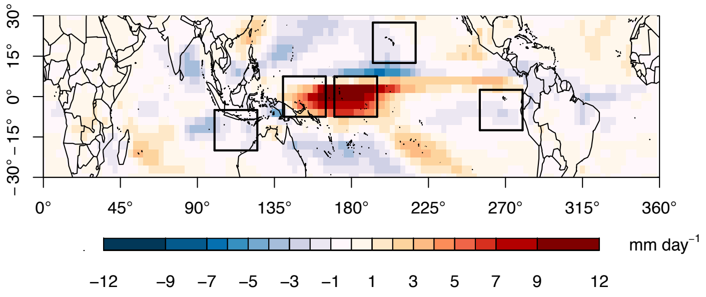

Figure 5. The same as Figure 4 but for CAM output.

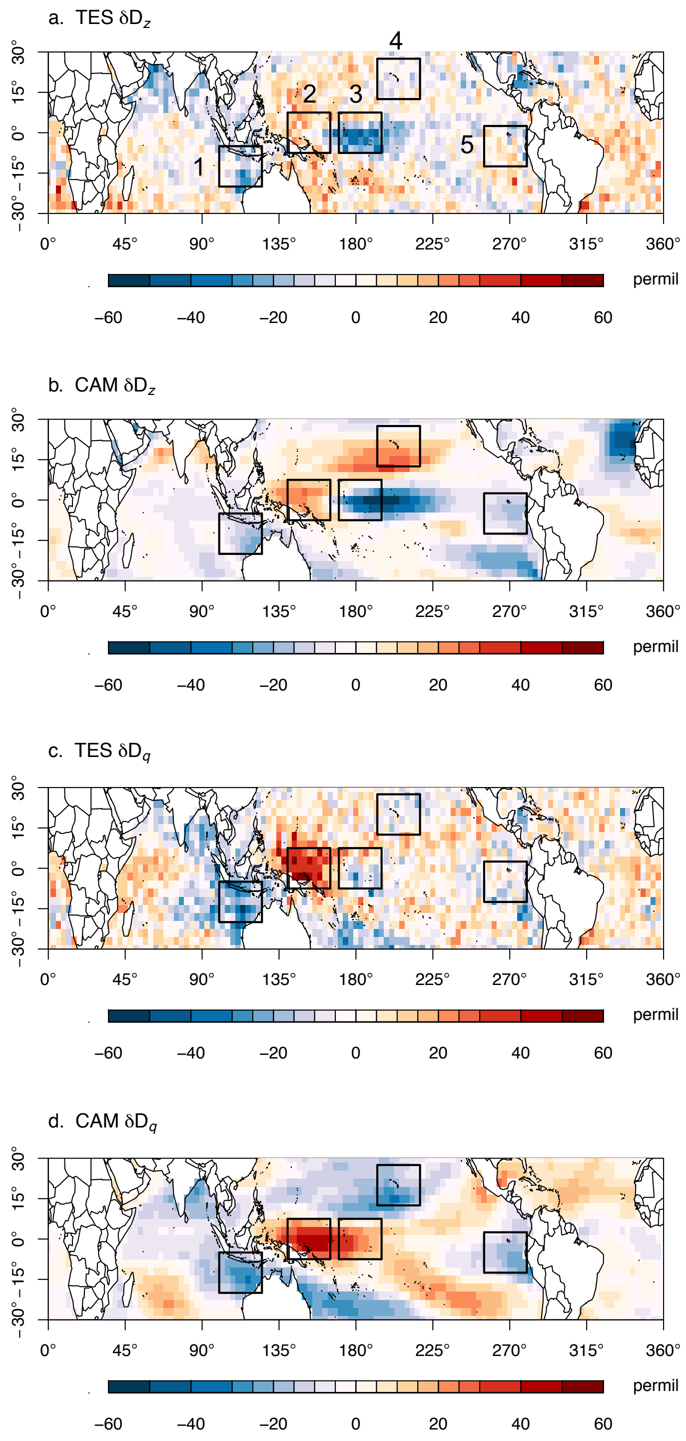

Figure 6. Changes in water vapor isotope ratios with ENSO. Composite differences in (a) TES 800-500-hPa layer mean δD (δD_z), (b) CAM 800-500-hPa layer mean δD (δD_z), (c) TES δD_q, and (d) CAM δD_q for cold minus warm phases of ENSO.

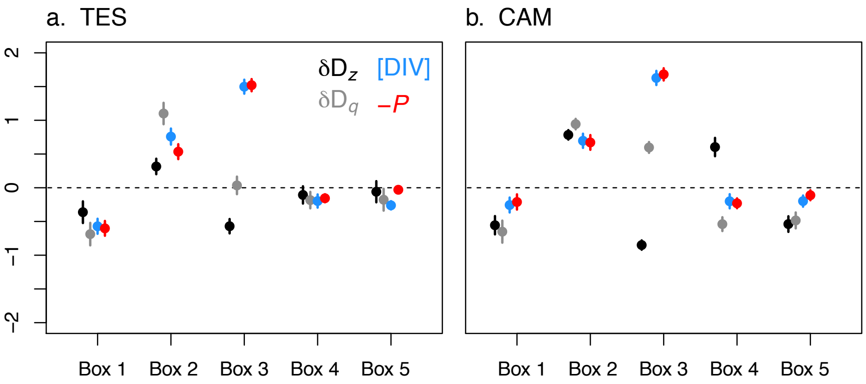

Figure 7. Mean standardized departures in δD_z (black), δD_q (gray), [DIV] (blue), and –*P* (red) between cold and warm phases of ENSO for the five boxed regions in Figs. 3-6. Panel (a) shows isotopic values from TES and estimates of [DIV] and -*P* from ERA, while (b) shows model-derived variables from CAM. Vertical lines represent 95% confidence intervals. Due to the large spatial correlation between variations in [DIV] and *E-P* with ENSO, only [DIV] is shown.

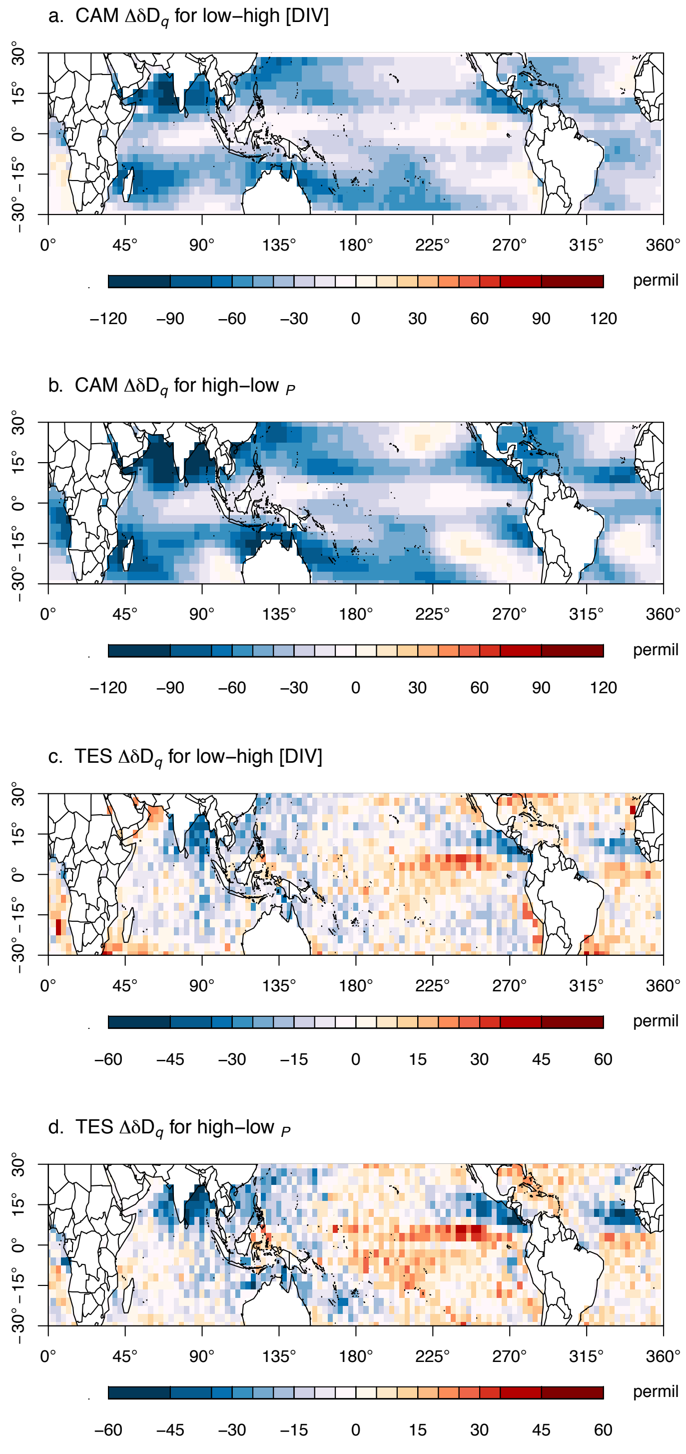

Figure 8. Changes in δD$_q$ with [DIV] and P, irrespective of the phase or strength of ENSO.

Composite differences in (a, b) CAM and (c, d) TES δD$_q$ for periods of high and low (a, c) [DIV] or (b, d) precipitation. As described in the Methods, high and low periods are defined by days in which each variable is in the top or bottom quartile of its distribution for the full Sept. 2004 – Dec. 2011 analysis period at a particular grid point. Equivalent composite differences in δD_q for periods of high and low *E-P* are provided in the Supporting Information. Notice that the scale for the TES composites is half the scale of the CAM composites.

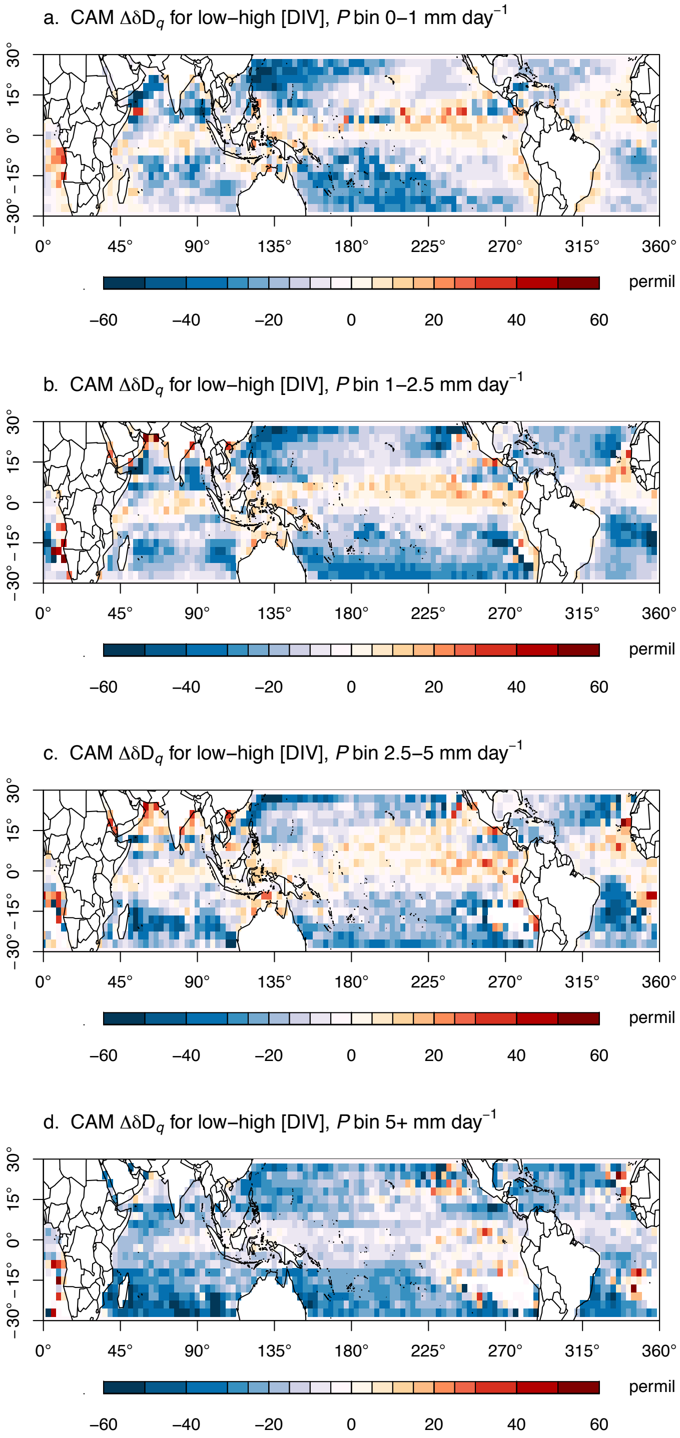
a. CAM $\Delta\delta D_q$ for low–high [DIV], P bin 0–1 mm day^{-1}

b. CAM $\Delta\delta D_q$ for low–high [DIV], P bin 1–2.5 mm day^{-1}

c. CAM $\Delta\delta D_q$ for low–high [DIV], P bin 2.5–5 mm day^{-1}

d. CAM $\Delta\delta D_q$ for low–high [DIV], P bin 5+ mm day^{-1}

Figure 9. Changes in δD_q with [DIV] when P is held constant. Composite differences in CAM δD_q for periods when [DIV] is in the top or bottom quartile of its distribution at each grid point and P falls within the following precipitation bins: (a) 0-1 mm day^{-1}, (b) 1-2.5 mm day^{-1}, (c) 2.5-

5 mm day^{-1}, and (d) 5+ mm day^{-1}. Equivalent composite differences in δD_q for periods of high and low E-P are provided in the Supporting Information

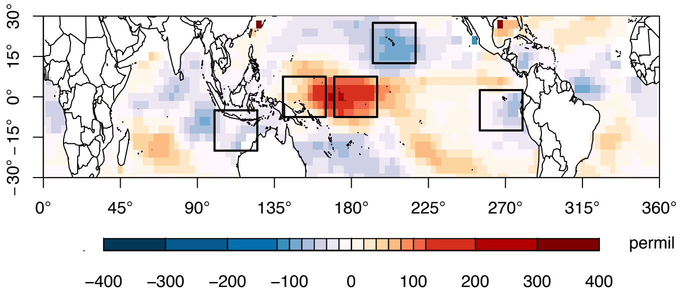
a. CAM δD Condensate

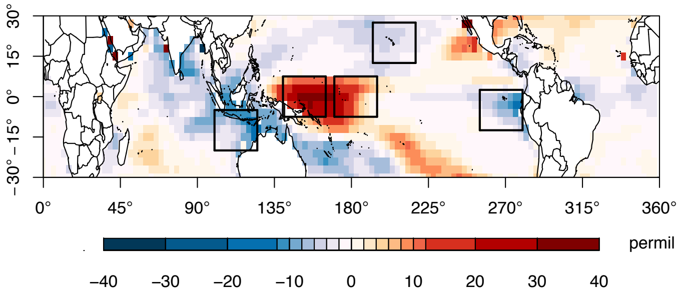
b. CAM δD Precipitation

Figure 10. Composite differences in the δD of (a) total column condensate and (b) precipitation, estimated from CAM, for cold minus warm phases of ENSO.

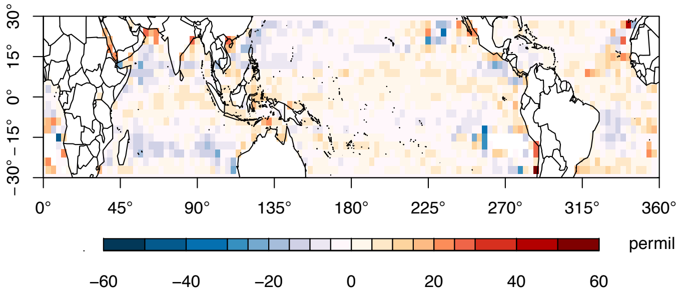

Figure 11. Composite differences in CAM δD_z when [DIV] is in the top or bottom quartile of its distribution at each grid point and *P* is between 2.5-5 mm day^{-1}. Compare with Fig. 9c.